Systematic Design and Modeling of a OTA-C Filter for Portable ECG Detection

Shuenn-Yuh Lee, *Member, IEEE*, and Chih-Jen Cheng, *Student Member, IEEE*

***Abstract*—This study presents a systematic design of the fully differential operational transconductance amplifier-C (OTA-C) filter for a heart activities detection apparatus. Since the linearity and noise of the filter is dependent on the building cell, a precise behavioral model for the real OTA circuit is created. To reduce the influence of coefficient sensitivity and maintain an undistorted biosignal, a fifth-order ladder-type lowpass Butterworth is employed. Based on this topology, a chip fabricated in a 0.18-μm CMOS process is simulated and measured to validate the system estimation. Since the battery life and the integration with the low-voltage digital processor are the most critical requirement for the portable diagnosis device, the OTA-based circuit is operated in the subthreshold region to save power under the supply voltage of 1 V. Measurement results show that this low-voltage and low-power filter possesses the HD3 of −48.9 dB, dynamic range (DR) of 50 dB, and power consumption of 453 nW. Therefore, the OTA-C filter can be adopted to eliminate the out-of-band interference of the electrocardiogram (ECG) whose signal bandwidth is located within 250 Hz.**

***Index Terms*—Continuous-time filter, ECG, low power, nonideality, nonlinearity, portable circuits, SIMULINK, subthreshold.**

I. Introduction

With the help of the integrated circuit technology, medical diagnostic instruments can be compacted to portable devices for the purpose of homecare to diagnose heart disease [1]. This can be done by creating an apparatus which simultaneously records electronic signals from the surface electrodes on the human body. These assistant technologies are not only used to diagnose patients, but also provide them access to handy and convenient medical instruments. Hence, the power-saving requirements of portable and durable equipment give circuit designers the impetus to reduce the current it consumes and extend the battery lifetime [2]. In addition to the issue of power consumption, the analog front-end circuits as the interface between physical signals and digital processor must operate under a low-supply voltage for the purpose of being integrated into the low-voltage system-on-a-chip (SoC) system [3], [4].

To preprocess the cardiac signal (also called ECG measured on the surface of the body), referring to Fig. 1, a preamplifier with low input-referred noise will be utilized to perform the 10–100 times amplification of the weak ECG signal (amplitude range of 100 μV–4 mV) [5]. Behind the amplifier, an ultra-low power filter with low cut-off frequency is adopted to decrease the out-of-band noise (typically above the frequency of 250 Hz [5]). However, for low frequency biomedical applications, realizing lowpass filter circuits with large time constant ($\tau = RC$) under an acceptable capacitor's value (typically <10 pF for the realizable area in the circuit implementation) isn't an easy task. For instance, the ECG application ($1/RC \sim 250$ Hz) requires a resistance greater than 100 MΩ.

Switched-capacitor (SC) is a popular integrated circuit technique used in implementing this long-term ECG monitor system [6], [7]. Due to the leakage problem of the advanced process, the sample-hold circuits of the switch-based topologies are not suitable for applications requiring large time constant (of the order of millisecond or more). In order to overcome the leakage problem, the leakage-reducing mechanism is usually required in the switched-capacitor circuits [8]. Thus, there have been the proposal to use low-power continuous-time well-suited OTA-based filters composed of the open-loop OTA-C integrators [9]–[13] in which the devices are operated in the subthreshold region to realize a very low transconductance (G_m, typically of the order of a few nanoamperes per volt). In OTA-based circuits, the OTA will dominate the performance of the filter circuit, and the ratio of the capacitor to the small transconductance determines the time constant of OTA-C integrators.

When performing a systematic OTA-based filter design, two considerations must be taken into account: first, we determine the topology and the specification of the filter appropriate for the biomedical signal acquisition; second, with a chosen topology, we determine whether a given building cell used to construct this filter fulfill the requirement of such signal processing. The decision in the first consideration depends on the characteristics of the bio-signals, such as the bandwidth as well as the tolerance to distortion, and the second consideration must be estimated by a detailed analytical model of nonideal factors caused by the OTA. In the continuous-time filter design, total harmonic distortion (THD) and signal-to-noise ratio (SNR) are often used to inspect the performance of the whole filter circuit. The main impact on THD is the inherent linearity of OTA's transconductance because it induces the harmonic distortion (HD) to the filter system. In the low-frequency application, the flicker and thermal noise of OTA, especially the former, will be a severe

Manuscript received March 27, 2008; revised May 21, 2008 and July 31, 2008. First published January 06, 2009; current version published January 28, 2009. This work was supported by the Chip Implementation Center (CIC) and the National Science Council, Taiwan, under Grants NSC 96-2628-E-194-015-MY3, NSC 96-2220-E-194-008, and NSC 96-2220-E-194-012. This paper was recommended by Associate Editor K. Chakrabarty.

The authors are with the Electrical Engineering Department, National Chung Cheng University, Min-Hsiung Chia-Yi, 62107 Taiwan (e-mail: sylee@vlsi.ee.ccu.edu.tw; 92bobs@vlsi.ee.ccu.edu.tw).

Color versions of one or more of the figures in this paper are available online at http://ieeexplore.ieee.org.

Digital Object Identifier 10.1109/TBCAS.2008.2007423

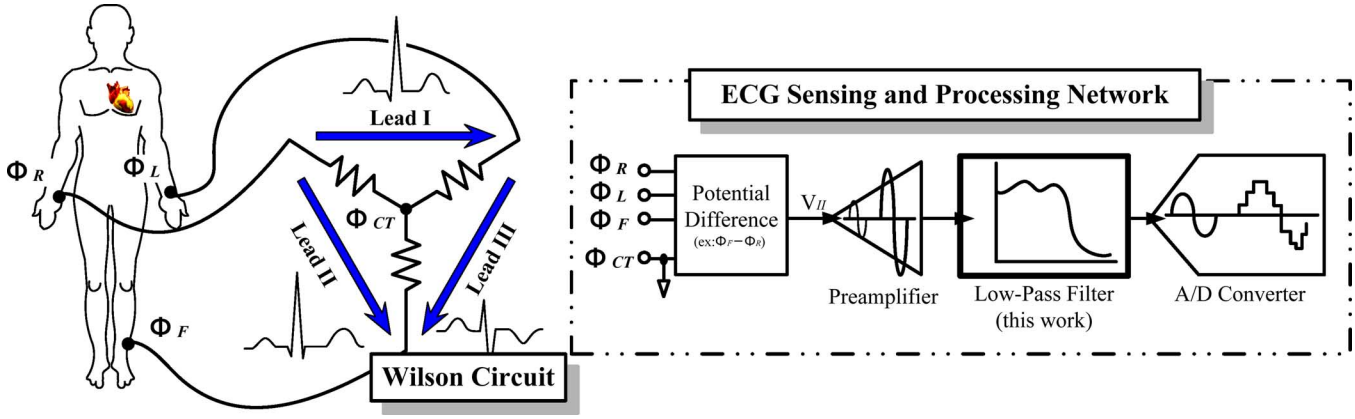

Fig. 1. Filter for a front-end circuits of portable ECG detection where Φ_{CT} means Wilson central terminal.

limitation of SNR. This would mean that a specified building cell must be well designed to meet the system requirement. In practice, the impact of linearity and noise are not captured until the integration of all circuits. Therefore, in order to estimate performance of the whole filter system by adopting a proper OTA in advance, there is a strong motivation for developing a systematic design flow of OTA-based filters that are capable of processing the low-frequency biophysical signals.

This paper presents a novel linearity and noise modeling approach for OTA and applies it to the OTA-C filter system. In practice, OTA's artifacts like nonlinear transconductance and its intrinsic noise can be described as behavior models to construct the basic block for a faster simulator, such as MATLAB or SIMULINK. In such fast simulators, the defections of OTA will produce some deviations of the output from the original input signal in the time domain. As a result, the evaluation of the system performance can be made through the power spectrum after fast Fourier transform (FFT) in the frequency domain. Corresponding to those relative characteristics from the system simulator, a 1-V OTA-C filter for ECG detection system as an example will be analyzed and discussed to demonstrate the presented model.

In Section II, the OTA's nonideal effects including nonlinearity, noise, and finite gain are discussed. Section III introduces the characteristics of a filter suitable for ECG signal detection. The nonideal model of OTA and its third harmonic distortion are presented in Section IV to assist the filter design. In Section V, the chip measurements including the AC signal testing, output noise measurement and an arrhythmia ECG tracing are made along with a brief comparison between the system and real circuit. Finally, Section VI briefly concludes this paper and compares with the previous works.

II. OTA Nonidealities

A first-order passive *RC* is shown in Fig. 2(a), where the series resistor with voltage source is transformed as a shunt resistor together with a current source according to the Norton's theorem. To realize an active filter, the passive components can be replaced by real OTA's circuits as illustrated in Fig. 2(b) which includes an input voltage-to-current transducer and an equivalent grounded resistor of OTA based on the close-loop configuration (for simplicity of illustration, the simple and single-ended configuration is adopted. However, the real circuit is implemented with a fully differential structure). Its transfer function is depicted as

$$\frac{V_{\text{out}}}{V_{\text{in}}} = -\frac{G_{m1}}{sC_L + G_{m2}} \tag{1}$$

The nonideal models of OTA, including nonlinearity, intrinsic noise and finite gain, will be developed to assist the performance analysis of the first-order filter. The details will be described in the following subsections.

A. OTA Nonlinearity

In the OTA of Fig. 2(b), many nonlinear effects are observed, such as nonlinear output current dependent on differential input pairs, finite output resistance of current sink/source. Therefore, it is difficult to estimate the system performance in advance without the nonlinear model. In conventional OTA design approach, the transfer characteristic between the transconductance and input differential voltage is of critical importance, as shown in Fig. 3. Its intrinsic nonlinearity can be calculated by the hand analysis and usually adopted to present the linearity of OTA [14], [15]. In general, a nonlinear transconductance is expressed as

$$G_m = G_{m0}\left(1 + \alpha_1 v_d + \alpha_2 v_d^2 + \ldots\right) \tag{2}$$

where G_{m0} is the transconductance of the OTA as the differential input voltage v_d equal to zero, and α_{i} represents the coefficient with respect to the higher order expansion term of nonlinearity. In order to observe how the distortion contributes to the system, the approximate model of OTA is adopted and the equivalent output resistance of OTA is assumed to be constant and signal independent. Consequently, the nonlinear behavioral model can be developed by SIMULINK building blocks as illustrated in Fig. 4, where af1 and af2 corresponding to the coefficient α_1 and α_2 in (2), respectively, which can be extracted from circuit behavior and using the curvefitting method.

B. OTA Noise

In practice, there are two main noise sources that influence the performance of OTA, such as flicker and thermal noise. The

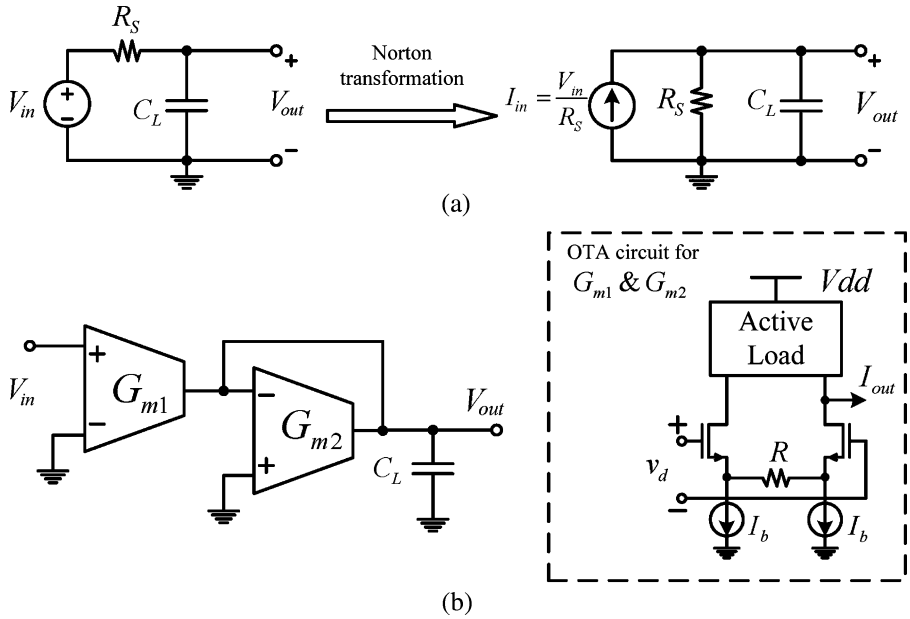

Fig. 2. Schematic of a first-order filter. (a) Passive *RC* network. (b) Active OTA-C realization with the source-degeneration OTA.

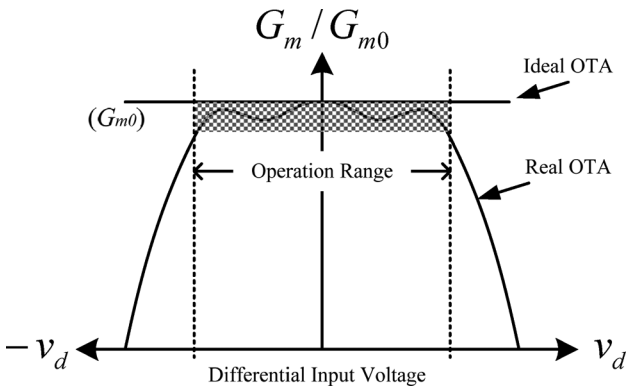

Fig. 3. A typical small-signal transconductance versus differential input voltage.

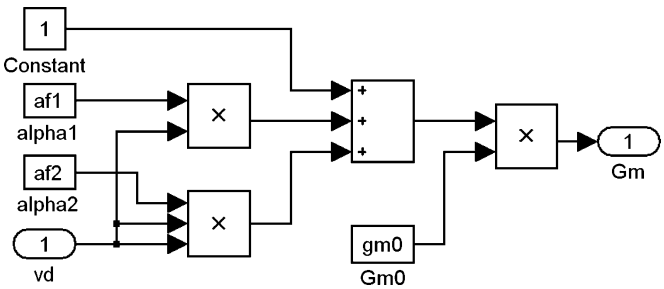

Fig. 4. Nonlinear transconductance model.

flicker noise in low-frequency band specifically influences the performance of small-G_m OTA. Both of them are taken into account when performing the circuit simulation. The flicker noise is also known as $1/f$ noise, because its noise power spectral density is inversely proportional to frequency. According to the general noise equation under NLEV $= 2$ in HSPICE [16], the input referred $1/f$ noise power spectrum density (PSD) with the unit of V^2/Hz is derived as

$$S_{f,\text{in}} = \frac{KF}{C_{\text{OX}} \cdot W_{\text{eff}} \cdot L_{\text{eff}} \cdot f^{AF}} \tag{3}$$

where the parameters KF and AF represent the coefficient and exponent constant of flicker noise, respectively, C_{ox} is the oxide capacitance per unit area, and W_{eff} and L_{eff} are the effective channel width and length of transistors, respectively. Moreover, the PSD equation of input-referred thermal noise can also be expressed as

$$S_{\text{th,in}} = \frac{4 \cdot \gamma \cdot k \cdot T}{G_m} \tag{4}$$

where k is Boltzmann's constant, T is the absolute temperature. In order to satisfy the low-power and low-frequency requirements of the OTA-C filter, most transistors of the OTA have to operate in the subthreshold regime. Thus, the value of γ is chosen as $1/(2\kappa)$ for subthreshold operation. Note that κ has a typical value of 0.7 and is equal to $1/n$, where n is a slope factor [17], [18].

For system simulation, time-domain emulated sources of $1/f$ and thermal noise can be approximated by considering the noise PSD as the spectrum of the sum of N sine-waves with random phase ϕ_{i}, each has the power equal to the area of a slide of the PSD. Combining the amplitude of $1/f$ noise, a_f, with that of thermal noise, a_{th}, the total input-referred noise can be presented as

$$v_{n,\text{in}}(t) = \sum_{i=1}^{N} (a_{f,i} + a_{\text{th}}) \cdot \sin(2\pi f_i + \phi_i) \tag{5}$$

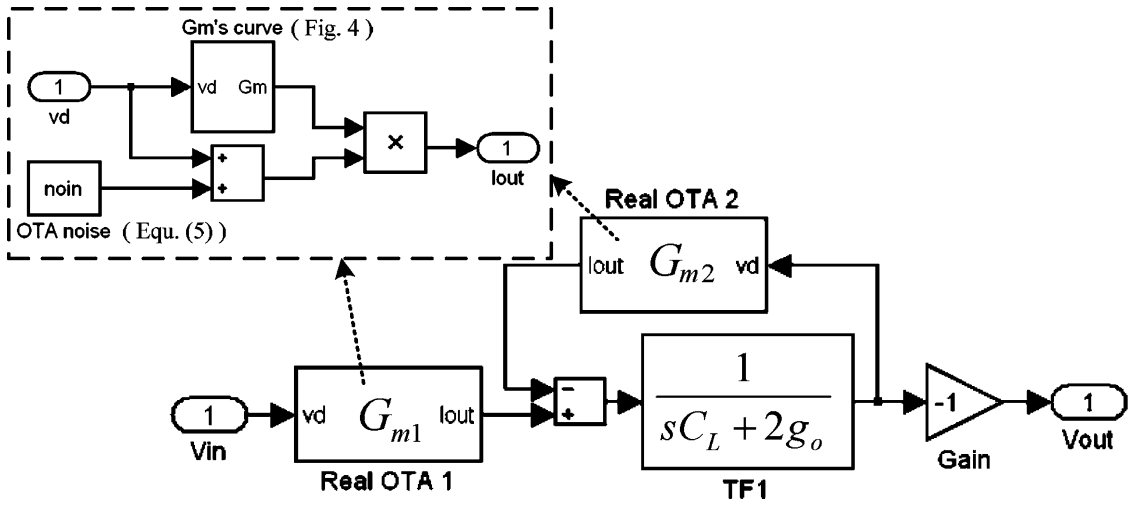

Fig. 5. SIMULINK model of a nonideal first-order filter.

where i denote the ith slide with respect to a specific frequency interval between f_i and $f_i + \Delta f$. In the case of $1/f$ noise, the coefficient $\alpha_{f,i}$ can be expressed as [19]

$$a_{f,i} = \sqrt{2\int_{f_i}^{f_i+\Delta f} S_f(f)df}. \tag{6}$$

For instance, in the ECG application with a limited bandwidth of 250 Hz, where the Δf is chosen as 1 Hz for simplicity, the N is equal to 250. Because the thermal noise can be assumed as white noise, its magnitudes are able to be derived directly in the following formula:

$$a_{\text{th}} = \sqrt{2S_{\text{th}}\Delta f}. \tag{7}$$

All mentioned noise power source could be evaluated precisely through a transistor-level simulator, such as HSPICE and PSPICE, to extract the quantitative data with respect to the frequency. Referring to (5), the total input referred noise is then superimposed to the nonlinear model of Fig. 4 and simulated in the time domain to find the circuit performance.

C. OTA Finite Gain

Equation (1) results from an assumption that the OTA has infinite output resistance. In the real circuit, however, a finite resistance due to the channel length modulation will result in larger integrator loss and further influence the filter response. Considering OTA output resistance $1/g_o$, the transfer function in Fig. 2(b) can be represented as

$$\frac{V_{\text{out}}}{V_{\text{in}}} = -\frac{G_{m1}}{sC_L + G_{m2} + 2g_o}. \tag{8}$$

With the three nonideal effects mentioned earlier, the behavioral model of Fig. 2(b) with SIMULINK tool can be developed, as shown in Fig. 5. The basic first-order filter will be integrated in the high-order filter design to estimate the system performance and to further acquire the circuit specifications according to the requirement of ECG diagnosis.

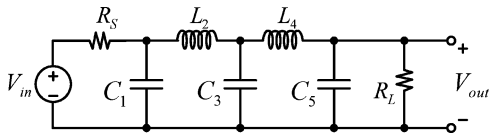

Fig. 6. Fifth-order passive butterworth filter.

III. Filter for ECG Detection

In order to precisely diagnose the heart disease, the detection circuits must be capable of attenuating the out-of-band interference and the noise before analog-to-digital converter to avoid the aliasing. For this reason, a fifth-order Butterworth filter with a maximum flat response and a cutoff frequency of 250 Hz are chosen for this design [5]. On the other hand, there must be a good enough inband performance for the filter to detect ECG signal precisely. The details are discussed as follows.

A. Filter Synthesis

Ladder type is a superior topology for a high-order filter because they are inherently insensitive to component variations, especially in their passband [20]. Hence, with the help of filter handbook, a fifth-order passive ladder-type filter is deduced as shown in Fig. 6. According to this circuit, the signal flow graph (SFG) mapping method can be utilized to generate an equivalent mathematical operation associated to the internal nodes. Consequently, the state equations of the filter can be derived, and thereby its ideal characteristics are able to be observed by the assistance of MATLAB. Fig. 7(a) shows the frequency response of this filter whose passband is flat and suitable for the undistorted ECG signal processing. Moreover, as depicted in Fig. 7(b), it possesses a nearly constant group delay below 150 Hz [21], where the most cardiac signals are located [22]. Based on the topology, a corresponding active circuit with the denormalized coefficients, as depicted in Table I, can be carried out through substituting the OTAs for these passive components.

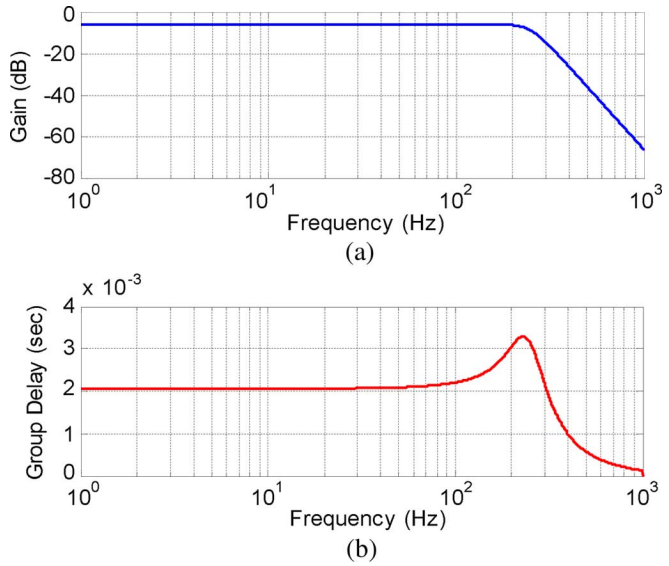

Fig. 7. Ideal filter characteristics of Fig. 6. (a) Frequency response with the cutoff frequency of 250 Hz. (b) The corresponding group delay.

TABLE I
COEFFICIENTS OF THE LOW-PASS BUTTERWORTH FILTER

	R_S & R_L	C_1 & C_5	C_3	L_2 & L_4
Normalized Coefficient	1	0.618	2	1.618
Denormalized Coefficient	R_0	$\frac{0.00395}{R_0}$	$\frac{0.00127}{R_0}$	$0.001*R_0$

B. Filter Performance

To inspect the filter performance, the dynamic range (DR, which is also defined as SNR with a specific THD) with safety margin for ECG detection can be driven as

$$\mathrm{DR}_{\min} = \mathrm{SNR}_{\min} = 20\log\frac{\mathrm{ECG}_{\max}}{\mathrm{ECG}_{\min}/2} \tag{9}$$

where $\mathrm{ECG}_{\max}$ and $\mathrm{ECG}_{\min}$ represent the maximum and minimum ECG signal level, respectively. Referring to the specification of ECG, the maximum and minimum signal levels are 4 mV and 100 μV, respectively. It indicates SNR must be larger than 38 dB (6.3 bits) in order to possess a good enough specification to process the ECG signals. On the other hand, the required input referred noise of the filter could be expressed as

$$\mathrm{Noi}_{\mathrm{in,ref}}(\mathrm{rms}) = \frac{V_{\mathrm{in,rms}}}{10^{\mathrm{SNR(dB)}/20}}. \tag{10}$$

As a result, the acceptable inband system noise can be determined with a specific input voltage under the required SNR. For instance, assuming an input voltage of 100 $\mathrm{mV_{pp}}$ and SNR of 38 dB, the input referred noise must be small than 445 $\mu\mathrm{V_{rms}}$. The next section will demonstrate, analysis, and model a good enough fifth-order filter for ECG detection.

IV. Circuit Implementation

A small-G_m OTA is adopted together with capacitors to implement the low-frequency filter [9]. This OTA possess two techniques including current cancellation as well as current division to reduce the transconductance. The pMOS is adopted in the input stage due to its low flicker noise that will be suitable for low-frequency application. Moreover, fully differential circuits are chosen due to a higher common-mode rejection and an increment of 3 dB in dynamic range rather than single-end structure.

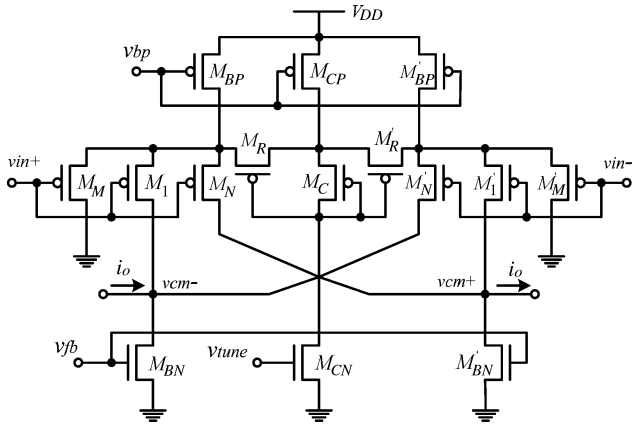

Fig. 8. Fully differential operational transconductance amplifier with vtune.

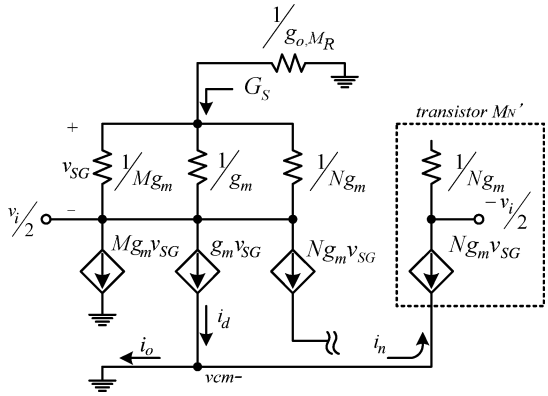

Fig. 9. Small-Signal circuit schematic for the source-degenerated OTA.

A. Linearized OTA Design

Fig. 8 shows the diagram of the adopted fully differential OTA which includes current division transistors M_M and current cancellation transistors M_N. Moreover, the transistor M_R is a source-degeneration device applied to improve the linearity. The transconductance ratio between M_M, M_N, and M_1 is M:N:1. For each transistor, the moderate inversion characteristic current I_S is given by [17]

$$I_S = 2\mu C_{\mathrm{OX}} n V_T^2 \cdot \frac{W}{L} \tag{11}$$

where μ is the carrier effective mobility in the channel, n is the subthreshold slope factor, and V_T is equal to kT/q, where q is the electron charge and T is the absolute temperature (at room temperature, V_T is about 25 mV). The ratio of channel current I_D to the moderate inversion characteristic current is defined as the inversion coefficient (IC)

$$IC = I_D/I_S. \tag{12}$$

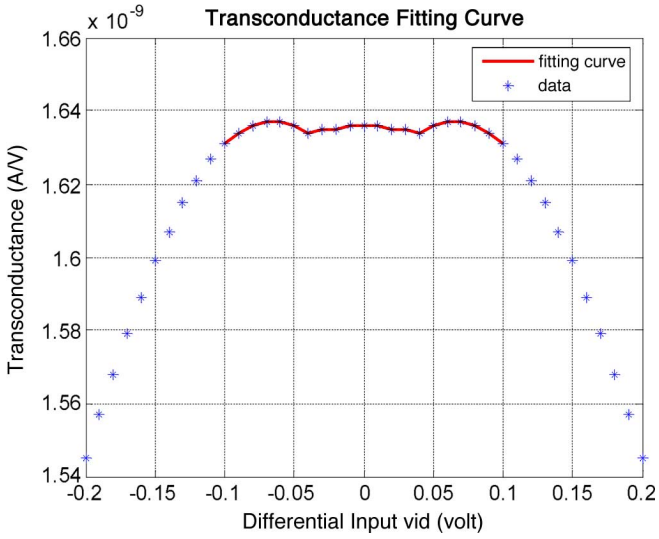

Fig. 10. Nonlinear G_m of the open-loop OTA.

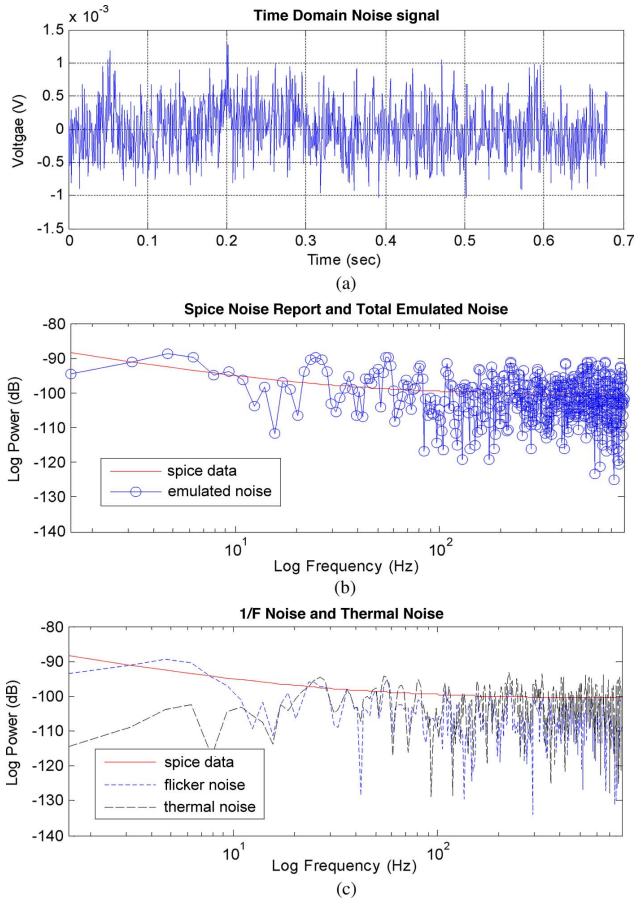

Fig. 11. Input-referred noise of the OTA. (a) Transient noise signal generated from the noise in the frequency domain. (b) HSPICE noise report versus total emulated noise. (c) Separation of $1/f$ noise from thermal noise.

If $10 > IC > 0.1$, the device operates in the moderate inversion region. Among the transistors of OTA, the devices, M_R and M'_R, are biased in the edge of moderate inversion and triode region to produce the linear transconductance for OTA. In addition, for a low-power concern, the other MOSFETs of this OTA are all designed with $IC < 0.1$ and operated in the subthreshold region. The channel current equation for these transistors is indicated as

$$I_D = I_0 \cdot e^{\frac{V_{GS}}{nV_T}} \cdot \left(1 - e^{\frac{-V_{DS}}{V_T}}\right) \tag{13}$$

with

$$I_0 = I_S \cdot \exp\left(\frac{-V_{th0} + (1-n)V_{SB}}{nV_T}\right)$$

where V_{SB} is the source-to-body voltage and V_{th0} is the threshold voltage at $V_{SB} = 0$. For drain-to-source voltage V_{DS} larger than $4V_T$, the channel length modulation has small impact on the output impedance. Hence, in the subthreshold operation, the V_{DS} of 150 mV are chosen for the transistors. The sources of three differential pairs are all connected to their respective bulks, leading to $V_{SB} = 0$. Therefore, the nonlinearity caused by body effect will be further diminished. In order to get a qualitative understanding of the G_m behavior in this OTA, the half circuit, which is composed of input stage formed by M_M, M_N and M_1 along with M_R and the other current division transistor M'_N, can be redrawn using small-signal equivalent circuit as depicted in Fig. 9, where the output resistances of the transistors are ignored and the transconductance can be approximated as

$$G_m = \frac{i_o}{v_{id}} = \frac{1-N}{1+N+M} \cdot \frac{G_S}{1 + G_S/g_{o,M_R}} \tag{14}$$

where G_S is the admittance looking into the source of input stage and equal to $(1+N+M)g_m$, and $g_{o,MR}$ represents the small signal drain-source conductance of M_R. For p-channel device, the corresponding first-order equation of $g_{o,MR}$ as the v_{SD} get close to $v_{DSAT}(= v_{SG} - V_{th})$ is given by

$$g_{o,M_R} = \mu_p C_{OX} \frac{W}{L}(v_{SG} - V_{th} - v_{SD}) \tag{15}$$

where the constant v_{SG} is provided by the self-biased transistor M_C. Furthermore, g_m in the subthreshold region can be driven from (13) as

$$g_m = \frac{I_D}{nV_T}. \tag{16}$$

In order to realize a very small transconductance, the denominator 1 + N + M is designed much larger than the nominator 1-N. On the other hand, from (15) and (16), the dimension and channel current can be scaled properly so that $g_m \gg g_{o,MR}$, which results in the unity-gain source-follower configuration composed of transistors M_M, M_N and M_1 along with the load resistor M_R, and thereafter the (14) can be further approximated as

$$G_m = \frac{i_o}{v_{id}} = \frac{1-N}{1+N+M} \cdot g_{o,M_R}. \tag{17}$$

From the above equation, g_{o,M_R} has direct influence on the linearity of the source-degenerated OTA. Since the devices M_R operate with the bulk connected to the power net, the $g_{o,MR}$ will suffer from linearity distortion due to the body effect. In

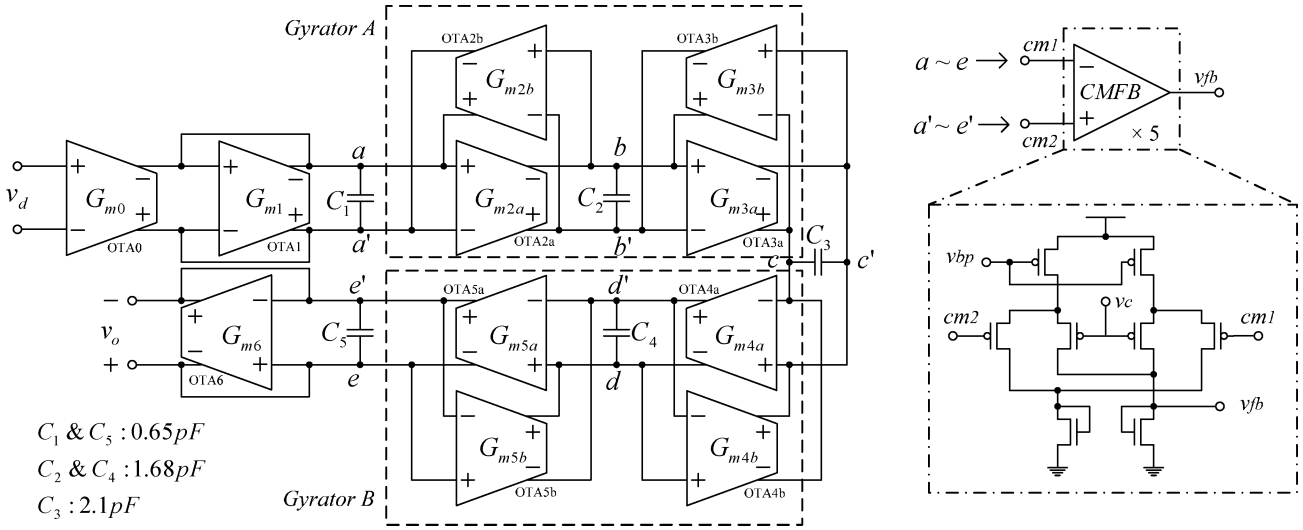

Fig. 12. Active circuit realization of fifth-order Butterworth filter.

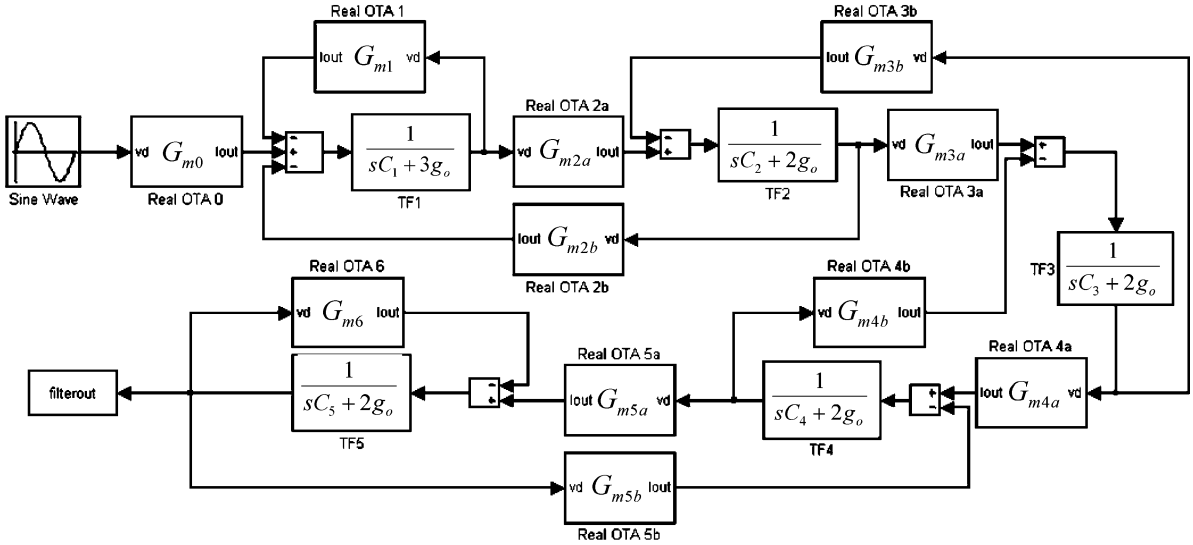

Fig. 13. Nonideal system model of the fifth-order filter.

addition, a little current deviation of the source-to-drain potential difference, $v_{\rm SD}$, will also induce high-order harmonic distortion. Consequently, the first-order (15) is not suitable for the analysis of small current in the order of nanoampere. In order to indicate how the nonlinear terms as depicted in (2) affect the transconductance of the OTA, the following p-channel's channel current equation valid for any potential change with respect to the ground is defined as [20]

$$i_D = \beta_p \left\{ \left(v_{\rm SG} - V_{\rm th0} - \frac{v_{\rm SD}}{2} \right) v_{\rm SD} - \gamma \cdot \sqrt{2|\phi_F|} \cdot v_{\rm SD} - \frac{2\gamma}{3} \cdot \left[(v_{\rm SD} + 2|\phi_F| - v_{\rm SB})^{\frac{3}{2}} - (2|\phi_F| - v_{\rm SB})^{\frac{3}{2}} \right] \right\} \quad (18)$$

with

$$\beta_p = \mu_p C_{\rm OX} \frac{W}{L}$$

where $\phi_{\rm F}$ represent the Fermi potential and is positive in p-channel devices, on the contrary, γ has a negative sign. A Taylor expansion relative to $v_{\rm SD}$ can be made with the derivatives of the 3/2 power term in (18). Thus, an infinite power series can be expressed as

$$i_D = \beta_p \left(\alpha_0 v_{\rm SD} + \alpha_1 v_{\rm SD}^2 + \alpha_2 v_{\rm SD}^3 + \ldots \right) \quad (19a)$$

where $\beta_p \alpha_0$ is the reciprocal of small-signal channel resistance, $r_{\rm ON}$, given by

$$r_{\rm ON} = \frac{L}{\mu_p C_{\rm OX} W (v_{GS} - V_{\rm th})} \quad (19b)$$

where $V_{\rm th}$ with the body effect is depicted as

$$V_{\rm th} = V_{\rm th0} + \gamma \left(\sqrt{2|\phi_F| - v_{\rm SB}} - \sqrt{2|\phi_F|} \right). \quad (19c)$$

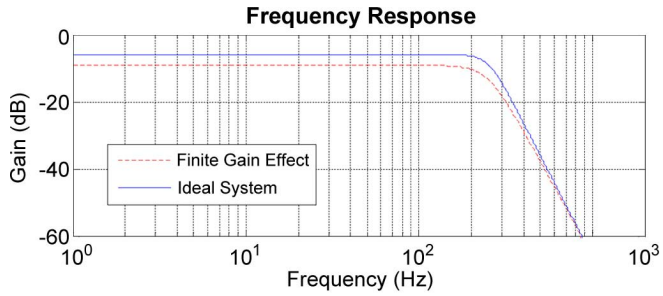

Fig. 14. Frequency response with the finite-gain effect.

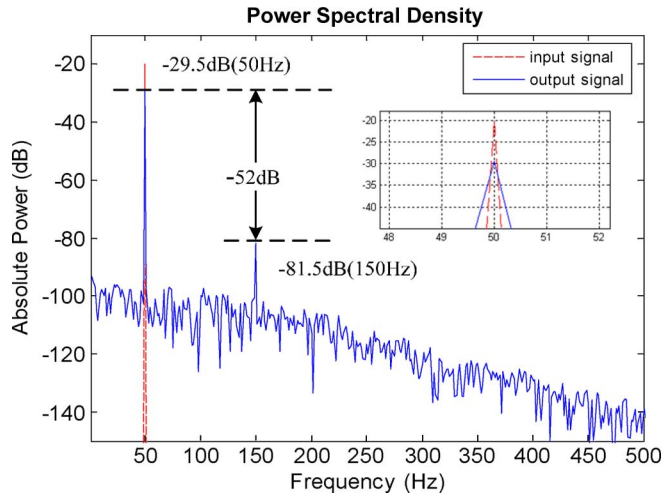

Fig. 15. Simulated output power spectrum of the fifth-order filter, where the subplot shows the gain degradation results from the finite-gain effect.

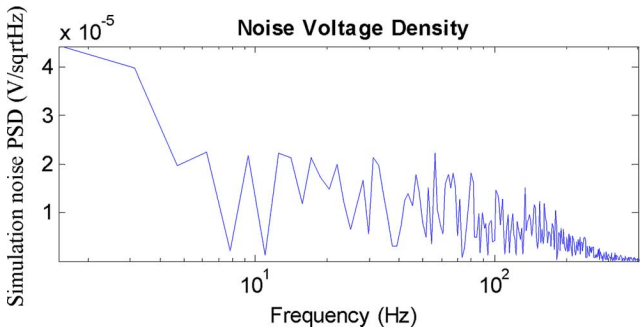

Fig. 16. Simulated output noise spectrum density of the fifth-order filter.

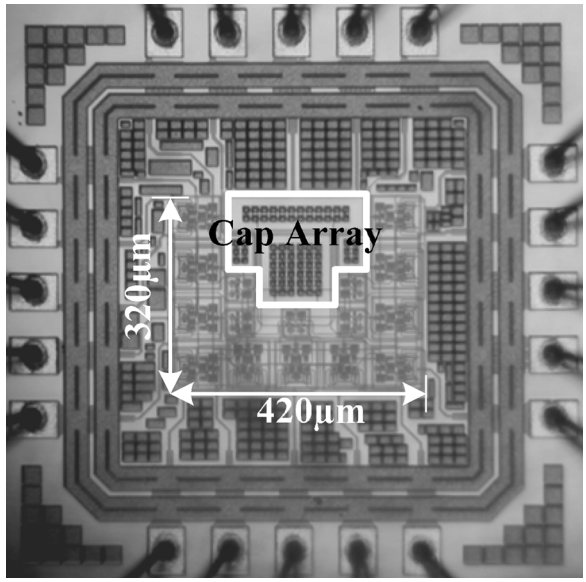

Fig. 17. Chip microphotograph of the OTA-C filter.

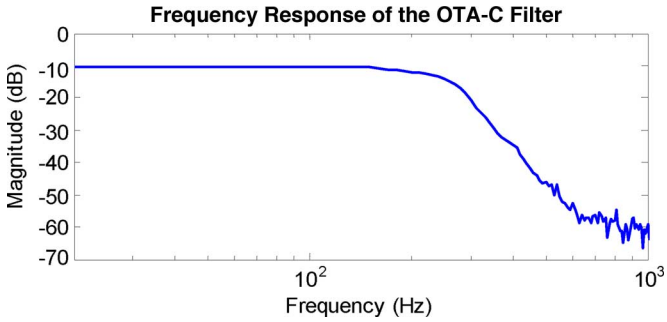

Fig. 18. Frequency response of the OTA-C filters.

Based on (18), the third harmonic distortion HD3 is specified as the ratio of the magnitude of the third power term to the level of the fundamental frequency, which suggests that

$$HD3 \cong \frac{\gamma \cdot v_{\mathrm{SD}}^2}{96(v_{\mathrm{SG}} - V_{\mathrm{th}})(2\phi_F - v_{\mathrm{SB}})^{\frac{3}{2}}}. \qquad (20)$$

In this OTA design, we take $\gamma = -0.49\ \mathrm{V}^{1/2}$, $2\phi_{\mathrm{F}} = 0.57$ V, and $V_{\mathrm{th0}} = 0.43$ V by consulting the HSPICE manual as well as the technology file. Moreover, $v_{\mathrm{SG}} = 0.57$ V and $v_{\mathrm{SB}} = 0.28$ V are available in the netlist report generated by HSPICE. Therefore, for this low voltage design, with the differential input voltage magnitude of 100 $\mathrm{mV_{pp}}$, the third harmonic distortion will be suppressed below -50 dB.

B. Matlab-Aided OTA Simulation

The simulated transconductance's data of the adopted differential low-G_m OTA is shown in Fig. 10, where the transconductance decreases abruptly as the output small-signal current is close to the bias current. When the differential input voltage v_{id} vary within ± 100 mV, the transconductance is almost constant with little nonlinear distortion. Referring to (2), for the purpose of emulating the nonlinear G_m, the fitting method is applied to this curve in the operation region, and thereby the G_{m0} is found to be 1.636 nS while α_2 is equal to 1.18 and $\alpha_1 \sim 0$ due to the symmetrical characteristic. Moreover, the quantitative input-referred noise associated to the OTA is obtained in the frequency domain from the ac analysis. This simulated data including flicker and thermal noise benefits to yield the time-domain noise source by (5)–(7), as shown in Fig. 11(a). Meanwhile, Fig. 11(b) and (c) show the power spectrum of the noise sources, where the total emulated noise energy is the sum of the flicker and thermal noise power, while the original spice data is also plotted to demonstrate the magnitude of the emulated noise source. Note that the zero decibel corresponds to the amplitude of 1 V for all the spectrums in this paper.

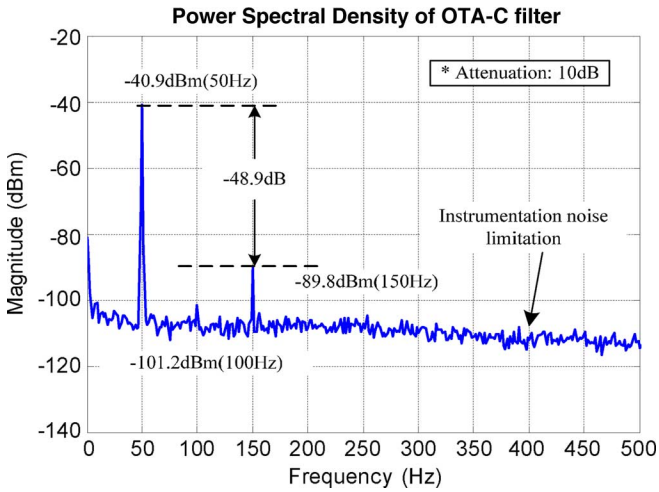

Fig. 19. Measured output power spectrum with a sinusoidal input signal of 50 Hz and 100 mV_{PP} with an attenuation of 10 dB.

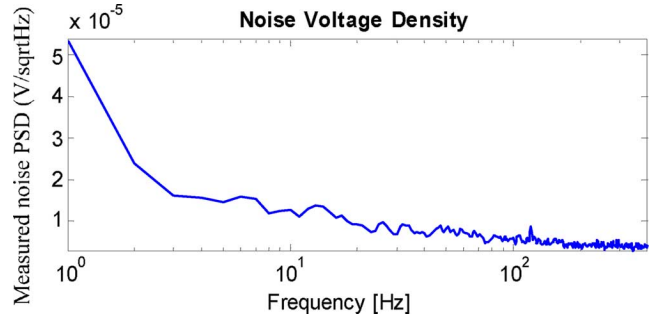

Fig. 20. Measured output noise spectrum density (average).

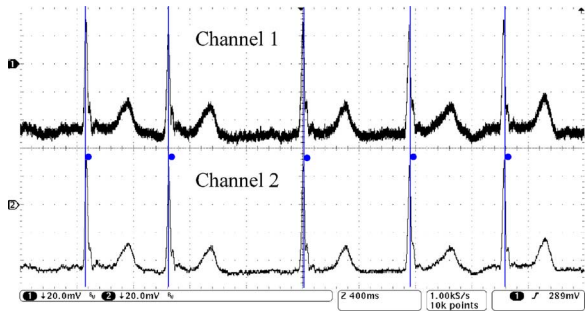

Fig. 21. Transient input/output of arrhythmic ECG.

C. Fifth-Order OTA-C Lowpass Filter Circuit

Referring to Fig. 12, the fifth-order OTA-C filter with common-mode feedback circuits was realized. The overall circuit consists of two grounded resistors G_{m0} and G_{m6}, five capacitors $C_1 \sim C_5$, and two gyrators A and B which are used to implement equivalently the inductors, L_2 and L_4, respectively. For the purpose of extending battery-life time, the filter with eleven OTAs shares five common-mode feedback circuits which sense the common output voltages of nodes $a \sim e$ in Fig. 12 and control the bias voltage vfb of the OTA as depicted in Fig. 8 to reduce power consumption.

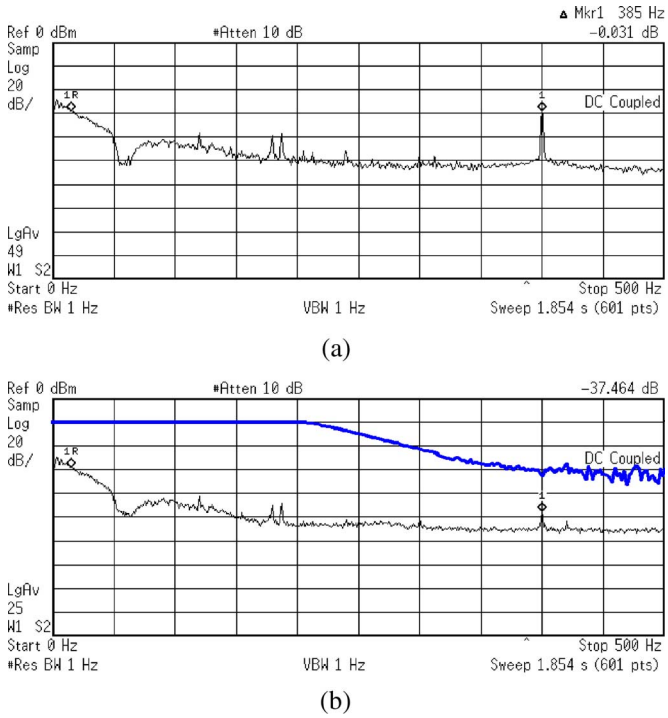

Fig. 22. Power spectrum of the real ECG signal. (a) Arrhythmic ECG with interference. (b) Interference attenuation by the OTA-C filter.

TABLE II
SUMMARY AND COMPARISONS OF THE OTA-C FILTER

	System Simulation	Measurement Results
Supply	—	1V
Power	—	453nW
Filter's order	5	5
DC Gain	-9.5dB	-10.5dB
Cutoff frequency	250Hz	~240Hz
HD3	-52dB	-48.9dB
Delay time(<150Hz)	~2ms	~2.5ms
Output Signal	-29.5dBm	-40.9dBm*
Noise floor	-72dB	-68dB

* Signal attenuation: 10 dB

D. Fifth-Order OTA-C Lowpass Filter Model

To evaluate the effect of the OTA nonidealities, all the integrators in Fig. 12 are replaced by the SIMULINK models as illustrated in Fig. 13. In this figure, the parasitic capacitors of all OTAs are ignored and the internal nodes a ∼ e absorb their surrounding admittances. Thus, it is beneficial to model these integrators simply as first-order transfer functions. Since the output noise is an uncorrelated random signal, the total time-domain noise source belongs to the differential OTA will be generated twice in MATLAB.

Fig. 14 shows the frequency response of this emulated system with the output resistance of the OTA equals to 9.53 GΩ. It can be clearly seen that the finite gain leads to a degradation of 3.5 dB to this filter over its passband. The transfer curve of this filter is also distorted due to the finite-gain impact on transfer function. Although these defections could be overcome by employing larger channel length or the technique of gain

TABLE III
SUMMARY AND COMPARISONS OF THE LOW-PASS OTA-C FILTER

	2000 [9]	2002 [10]	2004 [12]	2005 [13]	This work
V_{DD}	±1.5V	2.7V	1.25V	±1.5V	1V
Tech	CMOS 0.8μm	CMOS 1.2μm	FGCMOS 0.8μm	CMOS 0.35μm	CMOS 0.18μm
V_{th}	0.8V	0.9V	0.8V	0.6V	0.5V
Order	6(*S*)*[1]	2(*S*)	2(*S*)	5(*S*)	5(*D*)
BW	2.4Hz	0.3Hz	750Hz	37Hz	250Hz
THD	50dB	45dB (HD3)	48.5dB	49.7dB	48.6dB
DR	60dB	70.5dB	78dB	57dB	50dB
Power	10uW	8.18uW	2.5uW	11uW	453nW
Area	1mm^2	0.06mm^2 (off-chip cap)	0.23mm^2	0.25mm^2	0.13mm^2
NP*[2]	7.58x10^{-7}	8.42x10^{-7}	2.2x10^{-6}	7.64x10^{-7}	4.53x10^{-7}
NA*[3]	1.56	0.04	0.36	2.04	4.13
FoM1*[4]	2.10x10^{-9}	5.97x10^{-9}	1.42x10^{-8}	2.68x10^{-9}	1.81x10^{-9}
FoM2*[4]	1.04x10^{-7}	7.25x10^{-10}	4.32x10^{-6}	2.91x10^{-6}	1.87x10^{-6}

*1 (*S*): Single, (*D*): Differential.
*2 Normalized Power: $NP = Power \times (0.5/(V_{\rm DD} - V_{\rm th})) \times (1/V_{\rm DD})$.
*3 Normalized Area: $NA = Area/Tech^2$.
*4 $FoM1 = NP/(Order \times {\rm DR})$; $FoM2 = (Power \times BW \times NA)/(Order \times {\rm DR})$.

enhancement, this problem will become more severe with the scale-down process and lower supply voltage.

Finally, a transient sinusoidal wave with the amplitude of 0.1 corresponding to 100 $\rm mV_{pp}$ is injected into this system in order to inspect the linearity. Fig. 15 manifests the simulated power spectrum where the HD3 is −52 dB along with the noise floor of −72 dB within the passband of 250 Hz. This result is identical to the hand-analysis of the OTA's HD3 and demonstrates that the linearity limitation of this system, which mainly comes from the OTA circuit. On the other hand, the system output noise simulation result can be acquired by setting the input as zero, and consequently the output noise spectrum density is shown in Fig. 16, where the average input referred noise is below 300 $\mu \rm V_{rms}$.

V. MEASUREMENT RESULTS

The lowpass filter was fabricated in TSMC 0.18-μm 1P6M process with the metal–insulator–metal (MIM) capacitors. Since MIM capacitor has longer distance from the bulk than that of doubly poly process, the parasitic capacitor has less influence on frequency response. The active area occupies an area of 0.135 mm^2 (0.42 mm × 0.32 mm), as shown in Fig. 17. The floor plan of capacitors located at the center is symmetrical to reduce the effect of process variation. Moreover, in order to decrease the transconductance mismatch, the critical OTAs are placed as closely as possible to each other. For instance, the source and load equivalent resistors OTA 0, 1 and 6 are closely placed to each other to achieve the low-sensitivity design. This chip with 1-V supply voltage consumes 453 nA, in which the current of 308 nA is consumed by the 11 OTAs and the other current consumption is produced by common-mode feedback.

On the other hand, since the biomedical monitoring system is often with a programmable low-noise instrumentation amplifier prior to the antialias filter [23], the amplitude of the weak bioelectric signal will be amplified to a higher level before further processing. Therefore, the following tests are made under the assumption that the signal source had been amplified to the maximum input range of the filter with negligible noise and interference.

A. AC Signal Testing

A single external biasing voltage is applied to the *vtune* of the OTA of Fig. 8 to finely adjust the gate-to-source voltage of M_C leading to the change in transconductance which is used to compensate for the process variation. The measured transfer curve for this chip is shown in Fig. 18, where the cutoff frequency is degraded around 240 Hz and the dc gain is also declined to −10.5 dB, which demonstrates the nonideal effect due to the finite gain and the result is also in agreement with the system estimation.

A differential sinusoidal wave with a magnitude of 100 $\rm mV_{PP}$ and a frequency of 50 Hz is fed into the chip to measure the HD3 as shown in Fig. 19. It can be observed that the third harmonic is around 49 dB which is close to the system estimation, and the noise floor is −68 dB within the passband of 250 Hz. The out-of-band noise floor is much higher than that of system because of the instrumentation noise suffered from the active probe and the spectrum analyzer itself.

B. Output Noise Testing

As described in Section III, the integrated input referred noise must be below 445 $\mu \rm V_{rms}$ to achieve the minimum system requirement with an input voltage of 100 $\rm mV_{pp}$. Fig. 20 demonstrates the measured output noise which is identical to the system simulation noise as depicted in Fig. 16 and possesses an integrated input referred noise of 340 $\mu \rm V_{rms}$ to achieve an 8-bit resolution.

C. ECG Signal Testing

For convenience, an off-chip output buffer is added and configured to compensate this attenuation such that the following measurements of real signal could be observed appreciably. Hence, an arrhythmic ECG signal tracing [24] is adopted to

verify this function of our filter. By adding a distortion signal at the frequency of 400 Hz, an ECG signal with an emulated vibrating baseline could be generated as shown in channel 1 of Fig. 21, whose power spectrum is also revealed in Fig. 22(a). Note that this signal is amplified by the signal generator in advance. Because some tiny physical waves are covered, this kind of ECG signal will be inconvenient for the diagnosis of heart disease. With the help of our lowpass filter, the emulated 400 Hz harmonic could be attenuated magnificently and this filter behavior is depicted in Fig. 22(b), whose time-domain signal with a clear baseline is also shown in channel 2 of Fig. 21. Moreover, the time delay between the signals of channel 1 and channel 2 was measured to be $\sim$2.5 ms. Note that this fifth-order butterworth filter is configured as an inverting filter, so the signal in channel 2 is an inverting signal as well. Finally, the performance summary and the comparison between behavioral simulation and measured results of the OTA-C filter circuit are depicted in Table II.

VI. Conclusion

In this paper, we present a systematic design and modeling method for a low-voltage and low-power OTA-C filter to detect ECG signal. This method of building blocks in MATLAB SIMULIK environment contains some significant issues of the intrinsic properties of a real OTA, such as nonlinearity, noise, and finite gain. All the nonideal parameters can be added or removed independently with the system-level macromodel to help the designers to evaluate and observe the impact of real circuits on the whole system.

By the implementation of a lowpass OTA-C filter with a generic 0.18 μm CMOS technology, not only the hand-analysis of HD3 is identical to this system, but its measurement result validates the estimation environment as well. It is also revealed that the noise effect must be taken into account in the design instead of considering only the harmonic distortion, especially for a small physical electrical potential. With regards to the finite-gain effect, the resulting degradation of the inband response can be compensated in this detection system by the previous stage such as the preamplifer. A comparison between this work and the previous lowpass OTA-C filters under the similar THD is made in Table III. The results reveal that this chip has a good FoM under the model-based systematic design method.

This proposed set of models is suitable for the time-domain behavioral simulation of any OTA-based circuit design. In the future, the other nonlinearities could be considered into this model, such as finite bandwidth and the parasitics from the OTA, to further precisely obtain the required circuit specification.

Acknowledgment

The authors would like to acknowledge the measurement assistance given by K.-M. Huang and W.-C. Kao in the CBIC laboratory.

References

[1] B. Fuchs, S. Vogel, and D. Schroeder, "Universal application-specific integrated circuit for bioelectric data acquisition," *Med. Eng. Phys.*, vol. 24, pp. 695–701, 2002.

[2] K. Eshraghian, "SoC emerging technologies," *Proc. IEEE*, vol. 94, no. 6, pp. 1197–1213, Jun. 2006.

[3] T. B. Tarim and M. Ismail, "Enhanced analog "yields" cost-effective systems-on-chip," *IEEE Circuits Dev. Mag.*, vol. 15, no. 2, pp. 12–22, Mar. 1999.

[4] P. L. Levin and R. Ludwig, "Crossroads for mixed-signal chips," *IEEE Spectrum*, vol. 39, no. 3, pp. 38–43, Mar. 2002.

[5] J. G. Webster, *Medical Instrumentation: Application and Design*. New York: Wiley, 1995.

[6] L. Lentola, A. Mozzi, A. Neviani, and A. Baschirotto, "A 1- μA front end for pacemaker atrial sensing channels with early sensing capability," *IEEE Trans. Circuits Syst. II, Analog Digit. Signal Process.*, vol. 50, no. 8, pp. 397–403, Aug. 2003.

[7] K. Lasanen and J. Kostamovaara, "A 1-V analog CMOS front-end for detecting QRS complexes in a cardiac signal," *IEEE Trans. Circuits Syst. I, Reg. Papers*, vol. 52, pp. 2584–2594, Dec. 2005.

[8] L. S. Y. Wong, S. Hossain, A. Ta, J. Edvinsson, D. H. Rivas, and H. Nääs, "A very low power CMOS mixed-signal IC for implantable pacemaker applications," in *Proc. IEEE Solid State Circuits Conf.*, Feb. 2004, pp. 318–319.

[9] S. Solís-Bustos, J. Silva-Martínez, F. Maloberti, and E. Sánchez-Sinencio, "A 60 db dynamic-range CMOS sixth-order 2.4 Hz lowpass filter for medical applications," *IEEE Trans. Circuits Syst. II, Analog Digit. Signal Process. Conf.*, vol. 47, pp. 1391–1398, Dec. 2000.

[10] A. Veeravalli, E. Sánchez-Sinencio, and J. Silva-Martínez, "Transconductance amplifier structures with very small transconductances: A comparative design approach," *IEEE J. Solid-State Circuits*, vol. 37, no. 6, pp. 770–775, Jun. 2002.

[11] C. D. Salthouse and R. Sarpeshkar, "A practical micropower programmable bandpass filter for use in bionic ears," *IEEE J. Solid-State Circuits*, vol. 38, no. 1, pp. 63–70, Jan. 2003.

[12] E. Rodriguez-Villegas, A. Yúfera, and A. Rueda, "A 1.25-V micropower Gm-C filter based on FGMOS transistors operating in weak inversion," *IEEE J. Solid-State Circuits*, vol. 39, no. 1, pp. 100–111, Jan. 2004.

[13] X. Qian, Y. P. Xu, and X. Li, "A CMOS continuous-time lowpass notch filter for EEG systems," *Analog Integr. Circuits Signal Process.*, vol. 44, pp. 231–238, Jul. 2005.

[14] J. Silva-Martinez, M. S. J. Steyaert, and W. M. C. Sansen, "A large-signal very low-distortion transconductor for high-frequency continuous-time filters," *IEEE J. Solid-State Circuits*, vol. 26, no. 7, pp. 946–955, Jul. 1991.

[15] S. Koziel and S. Szczepanski, "Design of highly linear tunable CMOS OTA for continuous-time filters," *IEEE Trans. Circuits Syst. II, Analog Digit. Signal Process.*, vol. 49, no. 2, pp. 110–122, Feb. 2002.

[16] *"Star-HSPICE User's Manual,"* Avanti! Corp., Fremont, CA, Jun. 2002, Release 2002.2.

[17] Y. Tsividis, *Operation and Modeling of the MOS Transistor*, 2nd ed. New York: McGraw-Hill, 1998.

[18] E. A. Vittoz and J. Fellrath, "CMOS analog integrated circuits based on weak inversion operation," *IEEE J. Solid-State Circuits*, vol. 12, no. 6, pp. 224–231, Jun. 1977.

[19] N. H. Hamid, A. F. Murray, and S. Roy, "Time-domain modeling of low-frequency noise in deep-submicron MOSFET," *IEEE Trans. Circuits Syst. I*, accepted for publication.

[20] K. R. Laker and W. M. C. Sansen, *Design of Analog Integrated Circuits and Systems*. New York: McGraw-Hill, 1994.

[21] *Medical Electrical Equipment—Part 2-47: Particular Requirements for the Safety, Including Essential Performance, of Ambulatory Electrocardiographic Systems*, IEC 60601-2-47 Ed. 1.0 en:2001.

[22] J. D. Bronzino, *The Biomedical Engineering Handbook*, 2nd ed. Boca Raton, FL: CRC Press, 2000.

[23] K. A. Ng and P. K. Chan, "A CMOS analog front-end IC for portable EEG/ECG monitoring applications," *IEEE Trans. Circuits Syst. I, Reg. Papers*, vol. 52, no. 11, pp. 2335–2347, Nov. 2005.

[24] Chart-O-Matic: View Signals and Annotations, PhysioNet, created by MIT Room E25-505A [Online]. Available: http://www.physionet.org/cgi-bin/chart

Shuenn-Yuh Lee (M'98) was born in Taichung, Taiwan, in 1966. He received the B.S. degree from the National Taiwan Ocean University, Chilung, Taiwan, in 1988, and the M.S. and Ph.D. degree from National Cheng Kung University, Tainan, Taiwan, in 1994 and 1999, respectively.

Since 2002 and 2006, he has been an Assistant Professor and Associate Professor, respectively, at the Institute of Electrical Engineering, National Chung Cheng University, Chia-Yi, Taiwan. His present research activities involve the design of analog and mixed-signal integrated circuits including filter, high-speed ADC/DAC, and sigma-delta ADC/DAC, biomedical circuits and systems, low-power and low-voltage analog circuits, and RF front-end integrated circuits for wireless communications.

Dr. Lee now is a member of Circuits and Systems (CAS) Society, Solid-State Circuits Society, Communication Society, and Medicine and Biology Society of IEEE.

Chih-Jen Cheng was born in Taichung, Taiwan, in 1978. He received the B.S. degree in engineering science from National Cheng Kung University, Taiwan, in 2000. He is currently pursuing the Ph.D. degree from the Institute of Electrical Engineering, National Chung Cheng University, Chia-Yi, Taiwan.

His research interests include the design of low-voltage and low-power analog integrated circuits, and biomedical circuits and systems.